Discovery and Structure of a Potent and Highly Specific Blocker of Insect Calcium Channels*

Xiu-hong Wang‡, Mark Connor§, David Wilson¶, Harry I. Wilson□, Graham M. Nicholson□, Ross Smith, Denis Shaw‡‡, Joel P. Mackay§§, Paul F. Alewood¶, Macdonald J. Christie§, and Glenn F. King‡¶¶**

*From the ‡Department of Biochemistry, University of Connecticut Health Center, Farmington, Connecticut 06032, Departments of §Pharmacology and §§Biochemistry, University of Sydney, Sydney, New South Wales 2006, Australia, ¶Institute for Molecular Bioscience and **Department of Biochemistry, University of Queensland, Brisbane, Queensland 4072, Australia, □Department of Health Sciences, University of Technology, Sydney, New South Wales 2007, Australia, and ‡‡John Curtin School of Medical Research, Australian National University, Canberra, Australian Capital Territory 0200, Australia*

This work was supported by National Science Foundation Grant MCB9983242 (to G. F. K.), Australian Research Council grants (to G. M. N., M. J. C., and G. F. K.), and Postgraduate Research Scholarships (to X.-H. W., D. W., and H. I. W.).

The amino acid sequence reported in this paper has been submitted to the Swiss Protein Database under Swiss-Prot accession no. P82852.

The nucleotide sequence(s) reported in this paper has been submitted to the GenBank™ /EBI Data Bank with accession number(s) AF329442–AF329445.

The atomic coordinates and NMR restraints (code 1G9P and 1HP3) have been deposited in the Protein Data Bank, Research Collaboratory for Structural Bioinformatics, Rutgers University, New Brunswick, NJ (http://www.rcsb.org/).

The ^{1}H NMR chemical shifts for this protein are available in the BioMagResBank under BMRB accession no. 4923.

¶¶ To whom correspondence should be addressed: Dept. of Biochemistry, MC3305, University of Connecticut Health Center, 263 Farmington Ave., Farmington, CT 06032. Tel.: 860-679-8364; Fax: 860-679-1652; E-mail: glenn@psel.uchc.edu.

[1] The abbreviations used are: rpHPLC, reverse phase high pressure liquid chromatography; ACTX, atracotoxin; RACE, rapid amplification of cDNA ends; NOE, nuclear Overhauser enhancement; Aga, agatoxin; r.m.s., root mean square; NOESY, NOE spectroscopy; TOSCY, total correlation spectroscopy; ECOSY, exclusion correlation spectroscopy; PLTX, *Plectreurys tristes* toxin.

Abstract

We have isolated a novel family of insect-selective neurotoxins that appear to be the most potent blockers of insect voltage-gated calcium channels reported to date. These toxins display exceptional phylogenetic specificity, with at least a 10,000-fold preference for insect *versus* vertebrate calcium channels. The structure of one of the toxins reveals a highly structured, disulfide-rich core and a structurally disordered C-terminal extension that is essential for channel blocking activity. Weak structural/functional homology with ω-agatoxin-IVA/B, the prototypic inhibitor of vertebrate P-type calcium channels, suggests that these two toxin families might share a similar mechanism of action despite their vastly different phylogenetic specificities.

INTRODUCTION

New methods of insect control are urgently required due to the evolution of insect resistance to classical chemical pesticides (1), growing appreciation of the environmental damage caused by many agrochemicals, and increased public concern about the human health risks associated with prolonged insecticide exposure (2). One promising approach is to engineer plants to produce insect-specific toxins, as exemplified by the engineering of genes encoding insecticidal toxins from the soil bacterium *Bacillus thuringiensis* into a variety of agricultural cultivars (3). A potentially more selective method is to use insect-specific viruses as vectors to deliver toxins to a restricted number of target insects without harming non-target animals (4, 5).

Unfortunately, there are few well characterized peptide/protein toxins that lend themselves to these genomic approaches. Spider venoms can be viewed as preoptimized combinatorial libraries of insecticidal peptides, and therefore we decided to exploit these venoms in the search for *insect-specific* toxins suitable for engineering into plants and insect viruses. Here we describe a new family of insecticidal neurotoxins isolated by screening the venom of the lethal Australian funnel-web spider *Hadronyche versuta* (Fig. 1, *inset*). These toxins are the most potent blockers of insect voltage-gated calcium channels reported to date, but they are virtually inactive on vertebrate ion channels, making them ideal biopesticide candidates. The structure of one of the toxins reveals a compact, disulfide-rich core and a structurally disordered lipophilic extension that is essential for channel blocking activity.

EXPERIMENTAL PROCEDURES

Purification of Toxins—Funnel-web spiders were collected from the Blue Mountains west of Sydney (*H. versuta*), from Fraser Island, Queensland (*H. infensa*), and from the Illawarra region of New South Wales (*Atrax* sp. Illawarra). Lyophilized crude venom was fractionated using a Vydac C_{18} analytical reverse phase high pressure liquid chromatography (rpHPLC)[1] column as described previously (6). Semi-pure ω-ACTX-Hv2a obtained from this initial fractionation was further purified on the same column using a gradient of 30–48% acetonitrile over 35 min at a flow rate of 1 ml min^{-1}. Once purified to ~98% homogeneity, peptides were lyophilized and stored at –20 °C until further use. Cysteine residues were alkylated before sequencing (7).

Insect and Vertebrate Toxicity Assays—Insecticidal activity was tested by injecting peptides into house crickets (*Acheta domesticus* Linnaeus) as described previously (7). Vertebrate activity was assayed as described previously (8) using vertebrate smooth (vas deferens) and skeletal (biventer cervicis) nerve-muscle preparations; tissue contractions were recorded in the absence of additives or after injection of

peptides directly into the bath buffer. δ-Atracotoxin-Hv1a (100 nM), a modulator of voltage-gated sodium channels (9), was used as a positive control. Vertebrate toxicity was determined by subcutaneous injection of ω-ACTX-Hv2a in 0.1 ml of saline into young BALB/c mice (3.1 ± 0.2 g; $n = 3$). Toxicity was monitored over 72 h.

Preparation of cDNA Libraries and RACE Analysis—Venom glands were dissected from a single subdued specimen of *H. infens*a (mature female) and *Atrax* sp. Illawarra (mature male), and mRNA was immediately isolated using a QuickPrep Micro mRNA Purification Kit (Amersham Pharmacia Biotech). For the *H. infensa* mRNA template, first-strand cDNA synthesis employed Superscript II reverse transcriptase (Life Technologies, Inc.) to extend a 3' universal poly(dT) anchor primer (*Not*I-dT_{18}; Amersham Pharmacia Biotech). Second-strand synthesis used DNA polymerase I. Marathon adapters (CLONTECH) were then ligated to the cDNA ends. For the *Atrax* template, full-length single-stranded cDNAs were obtained by including a 5' SMART II oligonucleotide (CLONTECH) in addition to the *Not*I-dT_{18} primer.

5'-RACE of the *H. infensa* cDNA library employed a redundant primer based on the partial N-terminal sequence of mature toxin (5'-(AGTC)GT(AG)TT(AGTC)AC(AGTC)AC(AG)CA(AG)TC) and a 5' universal adapter primer (CLONTECH). Cloning and sequencing of the derived leader sequence allowed a gene-specific 3'-RACE primer (5'-gtggacgccATGAAATTTTCAAAGC) to be designed based on the 5'-untranslated region, translation start site, and N-terminal signal sequence. This gene-specific primer was used in conjunction with a 3' universal primer (Pacific Oligos) to amplify entire coding sequences from both the *H. infensa* and *Atrax* cDNA libraries. Final polymerase chain reaction products (450–470 base pairs) were purified, cloned, and sequenced.

Electrophysiology—Neurons were dissociated from brains of adult European honeybees (*Apis mellifera*) as described previously (6). Adult C57B16/J mice of either sex were anesthetized with halothane and then killed by cervical dislocation. Trigeminal ganglion neurons were isolated by gentle trituration of the minced ganglia after a 20-min treatment at 34 °C with papain (20 units/ml^{-1}) in a HEPES-buffered saline solution of 140 mM NaCl, 2.5 mM KCl, 2.5 mM $CaCl_2$, 1.5 mM $MgCl_2$, 10 mM HEPES, and 10 mM glucose, pH 7.3 (HBS).

Standard whole cell voltage clamp recordings (10) were made of bee brain calcium channel (I_{Ca}), sodium channel (I_{Na}), and potassium channel (I_K) currents and mouse sensory neuron I_{Ca} and I_{Na} at ambient temperature (22 °C–24 °C). For bee neurons, recordings were made with fire-polished borosilicate pipettes of ~6 megaohm resistance when filled with an intracellular solution of either of the following compositions: (*a*) 120 mM CsCl, 5 mM NaCl, 5 mM MgATP, 0.3 mM Na_2GTP, 10 mM EGTA, 2 mM $CaCl_2$, and 10 mM HEPES, pH 7.3 (for I_{Na} and I_{Ca}), or (*b*) 130 mM KF, 10 mM EGTA, 2 mM $CaCl_2$, and 10 mM HEPES, pH 7.3 (for I_K). For recordings of I_{Ca} and I_{Na}, the external solution consisted of 135 mM NaCl, 20 mM tetraethylammonium chloride, 5 mM CsCl, 5 mM $BaCl_2$, 10 mM HEPES, 10 mM glucose, and 0.05% bovine serum albumin, pH 7.3. For I_K recording, the external solution consisted of 130 mM NaCl, 20 mM KCl, 2.5 mM $CaCl_2$, 1.5 mM $MgCl_2$, 10 mM HEPES, 10 mM glucose, and 0.05% bovine serum albumin, pH 7.3. The same internal solution was used for recordings of mouse sensory neuron I_{Ca} and I_{Na}; electrodes had a resistance of 1–2 megaohms. I_{Ca} external solution contained 140 mM tetraethylammonium chloride, 2.5 mM $CaCl_2$, 2.5 mM CsCl, 10 mM HEPES, 10 mM glucose, and 0.05% bovine serum albumin, pH 7.3, whereas I_{Na} was recorded in HBS.

Neurons were voltage clamped at –90 mV, and currents were evoked by stepping the membrane potential from –60 to +60 mV. Toxin effects on I_{Ca} and I_{Na} were tested at the potential with the largest inward

current, usually –10 or 0 mV. In bee neurons, the peak inward currents were usually abolished by 100 μM Cd^{2+}, suggesting that the current was largely carried by Ca^{2+} channels. In a few bee neurons, there was a rapidly activating, transient, and Cd^{2+}-insensitive current that was blocked completely by tetrodotoxin (1 μM). In mouse sensory neurons, the peak inward currents evoked in the presence of potassium and sodium channel blockers were abolished by 30 μM Cd^{2+}. The inward currents recorded in HBS consisted of both tetrodotoxin-sensitive and tetrodotoxin-resistant components. Toxin effects on bee brain I_K were determined over a range of membrane potentials (from –40 to +60 mV). Data were collected and analyzed as described previously (11).

Folding and Purification of Truncated ω*-ACTX-Hv2a*—A synthetic peptide (90% purity) encompassing residues 1–32 of ω-ACTX-Hv2a was purchased from Auspep (Melbourne, Australia). The reduced peptide (referred to hereafter as CT-Hv2a) was oxidized/folded at ambient temperature (22 °C) in a glutathione redox buffer that promotes disulfide oxidation/shuffling (12). After 48 h, the reaction mixture was quenched with HCl and dialyzed against H_2O using 1-kDa cutoff cellulose dialysis tubing (Membrane Filtration Products) to remove folding buffer components. The lyophilized dialysate was dissolved in H_2O and then applied to a Vydac C_{18} analytical rpHPLC column; fully oxidized CT-Hv2a was eluted with a retention time of 19 min using a gradient of 22–47% acetonitrile over 30 min at a flow rate of 1 ml min^{-1}.

NMR Spectroscopy—NMR samples were prepared by dissolving 2.0 mg of ω-ACTX-Hv2a or 3.0 mg of synthetic CT-Hv2a in 260 μl of either 7.5% or 100% D_2O in a susceptibility-matched microcell (Shigemi) and then adjusting the pH to 4.71. NMR spectra were recorded at 288 K and 296 K using either a Bruker AVANCE or Varian INOVA 600 MHz spectrometer. The following two-dimensional spectra were recorded for both peptides in 7.5% D_2O: TOCSY (τ_m = 70 ms) and NOESY with τ_m = 60 ms (ω-ACTX-Hv2a, 296 K), 250 ms (ω-ACTX-Hv2a, 288 K), or 300 ms (ω-ACTX-Hv2a and CT-Hv2a, 296 K). The following two-dimensional spectra were recorded for the 100% D_2O samples: ECOSY (ω-ACTX-Hv2a only) and NOESY with τ_m = 300 ms.

Spectra were processed using XWINNMR (Bruker) or Felix97 (Molecular Simulations, Inc). Chemical shift assignments were made using XEASY (13) and have been deposited in BioMagResBank (BMRB accession code 4923). Hydrogen bonds were identified using hydrogen-deuterium exchange experiments (6).

Structure Calculations—NOESY cross-peaks were integrated in XEASY and converted to distance restraints (with pseudoatoms where appropriate) using CALIBA (14). Dihedral-angle restraints were derived as described previously (6). The intense intraresidue H_α–H_N NOE for Arg-26, combined with a $^3J_{HNH\alpha}$ value of ~7 Hz, allowed its ϕ angle to be restrained to 50 ± 40° for both peptides (15). H_β stereospecific assignments and χ_1 restraints for ω-ACTX-Hv2a were obtained using ECOSY-derived $^3J_{\alpha\beta}$ coupling constants in combination with H_α–H_β and H_N–H_β NOE intensities measured from the 60-ms NOESY spectrum. Proline H_β protons were stereospecifically assigned as described previously (6). All X-Pro peptide bonds were clearly identified as *trans* on the basis of characteristic NOEs (16). The disulfide bonding pattern was determined unequivocally from preliminary structure calculations.

The torsion angle dynamics program DYANA was used to calculate 5000 structures from random starting conformations. The best 100 structures (selected on the basis of final penalty-function values) were then refined in X-PLOR (17). The 20 lowest-energy X-PLOR conformers were used to represent the solution structures of ω-ACTX-Hv2a and CT-Hv2a. MOLMOL (18) was used for molecular graphics.

RESULTS

Isolation of a Novel Insecticidal Toxin—Fig. 1*a* shows a typical rpHPLC fractionation of crude venom from *H. versuta*. 50 fractions were individually assayed for insect and vertebrate toxicity. The late-eluting peak marked with an *arrow* caused immediate and sustained paralysis when injected into crickets (PD_{50} = 160 ± 9 pmol g^{-1}; mean duration of paralysis at a dose of 250–500 pmol g^{-1} = 4 –5 h). Injection of crickets with a second dose (250–500 pmol g^{-1}) of toxin before reversal of paralysis was lethal. The toxin was inactive in vertebrate smooth and skeletal nerve-muscle preparations at a concentration of 1 μM (data not shown). These two neuromuscular preparations were chosen for the vertebrate toxicity screen because in combination they contain most of the potential neuropharmacological targets of spider toxins such as ligand- and voltage-gated ion channels. As further evidence of its lack of vertebrate toxicity, the toxin did not cause any adverse effects when injected into newborn mice at doses of up to 800 pmol g^{-1}, which is 5-fold higher than the PD_{50} in crickets.

Proteolytic digestion combined with N- and C-terminal sequencing revealed the complete amino acid sequence of this 45-residue toxin (Fig. 1*b*). Consistent with its long rpHPLC retention time, the toxin contains an unusually high proportion (55%) of apolar residues, including a highly hydrophobic C-terminal tail. We named the peptide ω-ACTX-Hv2a (Swiss-Prot accession number P82852) based on its molecular target (see below) and published nomenclature rules (11). The toxin has no homologs in the protein/DNA sequence data bases.

Elucidation of Precursor Structure—A peptide with a rpHPLC retention time similar to that of ω-ACTX-Hv2a was also evident in the venom of *H. infensa*. However, despite several attempts, N-terminal sequencing yielded only 12 residues (GVLDCVVNTLGC), and C-terminal sequencing indicated that the peptide had a blocked C terminus. Hence, we used RACE analysis (19) to extract the complete mRNA sequences corresponding to this toxin using cDNA libraries prepared from the venom glands of *H. infensa* and *Atrax* sp. Illawarra (see "Experimental Procedures").

Sequencing of RACE-derived clones revealed two 306-base pair coding sequences from *H. infensa* (corresponding to two 102-residue translation products, ω-ACTX-Hi2a and ω-ACTX-Hi2b) and two 300-base pair coding sequences from the *Atrax* species (corresponding to two 100-residue translation products, ω-ACTX-As2a and ω-ACTX-As2b). The DNA sequences have been deposited in GenBank™ (GenBank™ accession numbers AF329442–329445). The derived amino acid sequences (Fig. 1*b*) indicate that these peptides are homologs of ω-ACTX-Hv2a and reveal that the mature toxins are obtained by processing of a much larger prepropeptide precursor. The propeptide cleavage site was readily discerned from the known N-terminal sequence of ω-ACTX-Hv2a and ω-ACTX-Hi2a, whereas the signal peptide cleavage site was predicted using SignalP (20).

The prepropeptide architecture is similar to that determined for conotoxins (21, 22) and provides the first circumstantial evidence that Australian funnel-web spiders have evolved a strategy similar to that of the cone snails for diversifying their toxin pool. The signal sequence is extremely well conserved (78% identity and 100% similarity if conservative substitutions are included; see Fig. 1*b*), whereas the mature peptide sequence is more diversified (53% identity). This finding is consistent with accelerated evolution (hypermutation) of the C-terminal region of the precursor to generate a library of functionally diverse toxins with identical cystine framework (21, 22). It will be interesting in future studies to directly examine whether the venom contains

families of functionally disparate toxins with the same signal sequence.

Mass spectral analysis of ω-ACTX-Hi2a (predicted oxidized mass = 4408 Da; observed mass = 4009 Da) indicated that it undergoes posttranslational deletion of the C-terminal four residues. C-terminal "trimming" has been noted for several spider (23, 24) and scorpion (25) toxins. The scorpion toxin AaH II from *Androctonus australis* Hector undergoes posttranslational cleavage at a C-terminal Gly-Arg followed by an amidation process that eliminates the C-terminal glycine (25). Similar processing at the C-terminal Gly-Arg sequence in the *H. infensa* toxins would yield a toxin with the experimentally observed mass and would explain the block encountered during C-terminal sequencing of ω-ACTX-Hi2a. Mass analysis of the *H. versuta* and *Atrax* toxins indicated that their C termini are not trimmed, consistent with the absence of the C-terminal Gly-Arg sequence.

ω-*ACTX-Hv2a Is a Potent and Specific Blocker of Insect Calcium Channels*—Application of ω-ACTX-Hv2a (10 pM to 100 nM) to bee brain neurons inhibited calcium channel currents (I_{Ca}) in all cells examined (n = 37; Fig. 2*a*), with maximum inhibition occurring at concentrations of >10 nM. The EC_{50} for ω-ACTX-Hv2a inhibition of I_{Ca} was ~130 pM (Fig. 2*c*). Inhibition was rapid at high concentrations and was not significantly reversed by prolonged washing (Fig. 2*d*). Application of ω-agatoxin (Aga)-IVA, the prototypic antagonist of vertebrate P-type voltage-gated calcium channels (26), also inhibited I_{Ca} in all bee neurons examined (n = 19), but the EC_{50} (10 nM) and the concentration required for maximum inhibition (>100 nM) were both significantly higher than those for ω-ACTX-Hv2a (Fig. 2*c*).

In striking contrast to its effect on invertebrate neurons, superfusion of high concentrations of ω-ACTX-Hv2a (1 μM; n = 10) for 5 min had little effect on I_{Ca} in mouse sensory neurons, whereas application of ω-Aga-IVA inhibited a component of I_{Ca} in all mouse sensory neurons with an EC_{50} of about 20 nM (maximum I_{Ca} inhibition ~40%; Fig. 2*c*). ω-ACTX-Hv2a (100 nM) did not inhibit the tetrodotoxin-sensitive I_{Na} of bee brain neurons (I_{Na} was 98 ± 4% of control; n = 4), nor did it significantly affect I_{Na} in mouse sensory neurons (I_{Na} was 97 ± 3% of control with ω-ACTX-Hv2a = 1 μM; n = 5). ω-ACTX-Hv2a (100 nM; n = 5) had no effect on bee brain I_K at any potential when neurons were stepped from –90 mV to between –40 and +60 mV.

We conclude that ω-ACTX-Hv2a is a potent and extremely specific blocker of insect voltage-gated calcium channels. Based on the data in Fig. 2*c*, we calculate that □-ACTX-Hv2a has at least a 10,000-fold preference for insect *versus* vertebrate calcium channels.

Three-dimensional Structure of ω-*ACTX-Hv2a*—The solution structure of ω-ACTX-Hv2a purified from *H. versuta* venom was determined using standard homonuclear NMR methods (16). The ensemble of structures (Fig. 3; Table I; Protein Data Bank accession code 1G9P) is highly precise with a backbone r.m.s. difference of 0.18 Å for the structured region (residues 3–32). According to PROCHECK (27), 75% of the non-Pro/Gly residues in the structured region lie in most favored sector of the Ramachandran plot, with the remaining 25% located in "additionally allowed" regions.

The disulfide-rich region of ω-ACTX-Hv2a (residues 3–32) is organized into a compact globular domain containing a small stretch of 3_{10}-helix (residues 13–17), a short β-hairpin (residues 23–30,

comprising β-strands at residues 23–25 and 28– 30), and well defined β-turns at residues 18–21 (type I) and 25–28 (type I') (Fig. 3*b*). This globular domain contains a small hydrophobic core formed by two buried disulfide bridges (17–29 and 11–24) and the side chain of Thr-21. In striking contrast to the highly ordered disulfide-rich core, the N-terminal two residues and the entire lipophilic C-terminal tail (residues 33– 45) are disordered in solution (Fig. 3*a*).

The three disulfide bridges in ω-ACTX-Hv2a form an inhibitory cystine knot motif (28) in which the Cys-17-Cys-29 disulfide passes through a 15-residue ring formed by the other two disulfide bridges and the intervening sections of polypeptide backbone (Fig. 3*b*). Although the N-terminal disulfide bridge of the inhibitory cystine knot motif does not generally contribute to the hydrophobic core of inhibitory cystine knot toxins and is not essential for formation of the basic inhibitory cystine knot fold (6, 29), a complete cystine knot motif has been found in all four atracotoxin structures reported to date (this study and Refs. 6, 9, and 11). Presumably, the additional stability and protease resistance conferred by the complete knot (28) are critical for effective delivery of these neurotoxins to their sites of action.

Structural/Functional Homology with ω-Agatoxin-IVA—A search of the protein structure database using DALI (30) revealed weak but functionally significant structural homology between ω-ACTX-Hv2a and ω-Aga-IVA from the unrelated American funnel-web spider *Agelenopsis aperta* (Fig. 4*a*). We previously noted close structural/functional homology between the sodium channel modifiers δ-ACTX from *H. versuta* and μ-Aga-I from *A. aperta* (6, 9). Given the large evolutionary distance between these arachnids (Australian funnel-web spiders are primitive mygalomorphs, whereas American funnel-web spiders are modern araneomorphs), these results imply a remarkable case of convergent evolution.

In addition to the significant structural homology between the disulfide-rich domains of ω-ACTX-Hv2a and ω-Aga-IVA, both toxins have an unstructured, lipophilic C-terminal extension that was demonstrated to be critical for the activity of ω-Aga-IVA (31). To examine the functional role of the unstructured C-terminal domain in ω-ACTX-Hv2a (*i.e.* residues 33– 45), we produced a synthetic peptide comprising only residues 1–32 of the parent toxin and determined its solution structure using NMR spectroscopy (Table I; Protein Data Bank accession code 1HP3). As expected, the truncated toxin has the same fold as the corresponding region of the full-length parent toxin (Fig. 4*b*). However, we found that the C-terminally truncated toxin did not inhibit insect calcium channels (Fig. 2*b*), nor did it competitively inhibit the activity of the native toxin (data not shown). Thus, we conclude that the lipophilic C-terminal extension is essential for interaction of ω-ACTX-Hv2a with insect calcium channels.

DISCUSSION

Insecticide Development—Most commonly used insecticides target voltage-gated sodium channels (*e.g.* DDT, pyrethroids), GABA receptors (*e.g.* cyclodienes and fipronil), or acetylcholinesterase (*e.g.* organophosphorus and carbamate insecticides) (32). This narrow target range has accelerated resistance development (1) and stimulated interest in the elucidation of new insecticidal compounds that act on novel targets. We have shown in this study that ω-ACTX-Hv2a acts on a nonconventional target, namely, insect voltage-gated calcium channels. Furthermore, this toxin appears to be the most potent blocker of these channels reported to date; its EC_{50} on bee brain neurons (~130 pM; this study) is significantly lower than that obtained for ω-

Aga-IVA on bee (~10 nM; this study) or cockroach (17 nM; Ref. 33) brain neurons.

The unprecedented phylogenetic specificity of ω-ACTX-Hv2a significantly augments its utility as a lead compound for insecticide development, with our studies indicating that the toxin has at least a 10,000-fold preference for insect over vertebrate calcium channels. Whereas the toxin was inactive in all vertebrates tested in this study (chicken, rat, and mouse), we have found that ω-ACTX-Hv2a is toxic to a wide range of insect orders, including Leptidoptera, Diptera, and Orthoptera (B. L. Sollod and G. F. King, unpublished results). PLTX-II appears to be the only peptide toxin with comparable potency on insect calcium channels (34), but its ion channel and phylogenetic specificity remains to be determined.

Mode of Action—Surprisingly, despite a complete lack of sequence similarity, we found that ω-ACTX-Hv2a has weak but functionally significant structural homology with ω-Aga-IVA/B from the American funnel-web spider *A. aperta*. Both toxins contain a highly ordered disulfide-rich core and an unstructured lipophilic C-terminal region that protrudes from this globular domain. Both toxins have markedly reduced activity when the lipophilic C-terminal extension is deleted. Furthermore, we demonstrated that C-terminally truncated ω-ACTX-Hv2a does not competitively inhibit the activity of the full-length toxin, suggesting that the disulfide-rich core does not bind the channel in the absence of the C-terminal tail. These results lead us to propose a possible model for the mode of action of these toxins.

It seems improbable that the structurally disordered C-terminal tails of ω-ACTX-Hv2a and ω-Aga-IVA make specific interactions with residues on the extracellular surface of voltage-gated calcium channels. First, it is difficult to envisage how these lipophilic tails could make extensive favorable contacts with the largely polar surface of the channel. Second, the C-terminal apolar tail of ω-ACTX-Hv2a is a low complexity sequence, comprising a triple (G/P)G(L/I)(L/V) repeat, which seems unlikely to make specific high-affinity contacts with the channel surface. Third, in this model, immobilization of the C-terminal tail upon channel binding would incur a huge loss of conformational entropy, which is difficult to reconcile with EC_{50} values in the picomolar range.

Thus, we suggest that ω-ACTX-Hv2a and ω-Aga-IVA share a similar mechanism of action in which the lipophilic tail does not make specific high-affinity contacts with the extracellular surface of the targeted calcium channel but rather *initiates* toxin binding by penetrating the membrane either adjacent to the channel or by intercalation between transmembrane segments of the channel protein (Fig. 4*c*). A similar model has been proposed for the mode of action of ω-Aga-IVB (35). Limited motion of the tail region within the membrane might minimize the loss of conformational entropy suffered by the toxin upon channel binding. We propose that anchoring of the C-terminal tail in the membrane somehow facilitates direct interaction of the disulfide-rich core region with the extracellular surface of the channel (*i.e.* the tail "targets" the structured region to the channel). One possibility is that binding of the C-terminal tail alters the channel conformation sufficiently to reveal a cryptic high-affinity binding site for the disulfide-rich portion of the toxin. In this model, C-terminal truncates would not be expected to bind the channel or act as competitive inhibitors of the wild-type toxin, which is what we observed experimentally.

While further experiments will clearly be required to test this hypothesis, it is salient to note that the insect calcium channel blocker PLTX-II from the spider *Plectreurys tristis* contains a C-

terminal palmitoyl group that is essential for biological activity (36), and therefore it may function similarly. Thus, it will be instructive in future experiments to examine whether the C-terminal tail of ω-ACTX-Hv2a can be replaced by nonspecific hydrophobic anchors such as a palmitoyl group.

Acknowledgments—We thank Drs. Mark Maciejewski, Roger Drinkwater, and Benjamin Oldroyd for help with NMR data acquisition, RACE analysis, and bee collection, respectively.

REFERENCES

1. Feyereisen, R. (1995) *Toxicol. Lett.* **82–83,** 83–90

2. Betarbet, R., Sherer, T. B., MacKenzie, G., Garcia-Osuna, M., Panov, A. V., and Greenamyre, J. T. (2000) *Nat. Neurosci.* **3,** 1301–1306

3. Shelton, A. M., Tang, J. D., Roush, R. T., Metz, T. D., and Earle, E. D. (2000) *Nat. Biotechnol.* **18,** 339–342

4. Cory, J. S., Hirst, M. L., Williams, T., Hails, R. S., Goulson, D., Green, B. M., Carty, T. M., Possee, R. D., Cayley, P. J., and Bishop, D. H. L. (1994) *Nature* **370,** 138–140

5. Bonning, B. C., and Hammock, B. D. (1996) *Annu. Rev. Entomol.* **41,** 191–210

6. Wang, X.-H., Connor, M., Smith, R., Maciejewski, M. W., Howden, M. E. H., Nicholson, G. M., Christie, M. J., and King, G. F. (2000) *Nat. Struct. Biol.* **7,** 505–513

7. Wang, X.-H., Smith, R., Fletcher, J. I., Wilson, H., Wood, C. J., Howden, M. E. H., and King, G. F. (1999) *Eur. J. Biochem.* **264,** 488–494

8. Szeto, T. H., Wang, X.-H., Smith, R., Connor, M., Christie, G. M., Nicholson, G. M., and King, G. F. (1999) *Toxicon* **38,** 429–442

9. Fletcher, J. I., Chapman, B. E., Mackay, J. P., Howden, M. E. H., and King, G. F. (1997) *Structure* **5,** 1525–1535

10. Hamill, O. P., Marty, A., Neher, E., Sakmann, B., and Sigworth, F. J. (1981) *Eur. J. Physiol.* **391,** 85–100

11. Fletcher, J. I., Smith, R., O'Donoghue, S. I., Nilges, M., Connor, M., Howden, M. E. H., Christie, M. J., and King, G. F. (1997) *Nat. Struct. Biol.* **4,** 559 –566

12. Fletcher, J. I., Dingley, A. J., Smith, R., Connor, M., Christie, M. J., and King, G. F. (1999) *Eur. J. Biochem.* **264,** 525–533

13. Bartels, C., Xia, T.-H., Billeter, M., Güntert, P., and Wüthrich, K. (1995) *J. Biomol. NMR* **5,** 1–10□14. Gu¨ntert, P., Mumenthaler, C., and Wüthrich, K. (1997) *J. Mol. Biol.* **273,**283–298

15. Ludvigsen, S., and Poulsen, F. M. (1992) *J. Biomol. NMR* **2,** 227–233

16. Wüthrich, K. (1986) *NMR of Proteins and Nucleic Acids*, John Wiley & Sons, Inc., New York

17. Brünger, A. T. (1992) *X-PLOR Version 3.1*, Yale University Press, New Haven, CT

18. Koradi, R., Billeter, M., and Wüthrich, K. (1996) *J. Mol. Graph.* **14,** 51–55

19. Frohman, M. A. (1993) *Methods Enzymol.* **218,** 340–356

20. Nielsen, H., Engelbrecht, J., Brunak, S., and von Heijne, G. (1997) *Protein Eng.* **10,** 1–6

21. Olivera, B. M., Hillyard, D. R., Marsh, M., and Yoshikami, D. (1995) *Trends Biotechnol.* **13,** 422–426

22. Olivera, B. M., and Cruz, L. J. (2001) *Toxicon* **39,** 7–14

23. Diniz, M. R., Paine, M. J., Diniz, C. R., Theakston, R. D., and Crampton, J. M. (1993) *J. Biol. Chem.* **268,** 15340–15342

24. Leisy, D. J., Mattson, J. D., Quistad, G. B., Kramer, S. J., Van Beek, N., Tsai, L. W., Enderlin, F. E., Woodworth, A. R., and Digan, M. E. (1996) *Insect Biochem. Mol. Biol.* **26,** 411–417

25. Bougis, P. E., Rochat, H., and Smith, L. A. (1989) *J. Biol. Chem.* **264,** 19259 –19265

26. Mintz, I. M., Venema, V. J., Swiderek, K. M., Lee, T. D., Bean, B. P., and Adams, M. E. (1992) *Nature* **355,** 827–829

27. Laskowski, R. A., MacArthur, M. W., Moss, D. S., and Thornton, J. M. (1993) *J. Appl. Crystallogr.* **26,** 283–291

28. Craik, D. J., Daly, N. L., and Waine, C. (2001) *Toxicon* **39,** 43–60

29. Le-Nguyen, D., Heitz, A., Chiche, L., El Hajji, M., and Castro, B. (1993) *Protein Sci.* **2,** 165–174

30. Holm, L., and Sander, C. (1993) *J. Mol. Biol.* **233,** 123–138

31. Kim, J. I., Konishi, S., Iwai, H., Kohno, T., Gouda, H., Shimada, I., Sato, K., and Arata, Y. (1995) *J. Mol. Biol.* **250,** 659–671

32. French-Constant, R. H., Pittendringh, B., Vaughan, A., and Anthony, N. (1998) *Philos. Trans. R. Soc. Lond. B. Biol. Sci.* **353,** 1685–1693

33. Benquet, P., Le Guen, J., Dayanithi, Y., Pichon, Y., and Tiaho, F. (1999) *J. Neurophysiol.* **82,** 2284–2293

34. Leung, H.-T., Branton, W. D., Phillips, H. S., Jan, L., and Byerly, L. (1989) *Neuron* **3,** 767–772

35. Yu, H., Rosen, M. K., Saccomano, N. A., Phillips, D., Volkmann, R. A., and Schreiber, S. L. (1993) *Biochemistry* **32,** 13123–13129

36. Branton, W. D., Rudnick, M. S., Zhou, Y., Eccleston, E. D., Fields, G. B., and Bowers, L. D. (1993) *Nature* **365,** 496–497

TABLE I *Structural statistics for the families of ω-ACTX-Hv2a and CT-Hv2a structures*

	ω-ACTX-Hv2a	CT-Hv2a
Experimental restraints		
Meaningful intraresidue distances ($i - j = 0$)	134	100
Sequential distances ($\|i - j\| = 1$)	173	134
Medium-range distances ($\|i - j\| = \leqq 5$)	55	48
Long-range distances ($\|i - j\| = > 5$)	66	63
Hydrogen bonds	24	22
Dihedral angles	37	21
Total	489	365
Mean r.m.s. deviations from experimental restraints		
NOE distances (Å)	0.0208 ± 0.0007	0.0291 ± 0.0005
Dihedral angles (degree)	0.147 ± 0.039	0.198 ± 0.049
Mean r.m.s. deviations from idealized covalent geometry[a]		
Bonds (Å)	0.00309 ± 0.00004	0.00317 ± 0.00004
Angles (degree)	0.406 ± 0.005	0.418 ± 0.004
Impropers (degree)	0.297 ± 0.009	0.303 ± 0.003
Mean X-PLOR energies (kcal/mol^{-1})		
E_{NOE}[b]	9.8 ± 0.6	15.5 ± 0.6
E_{cdih}[b]	0.049 ± 0.026	0.053 ± 0.025
E_{bond}	5.98 ± 0.16	4.61 ± 0.11
E_{improper}	9.41 ± 0.27	3.18 ± 0.07
E_{angle}	28.6 ± 0.8	22.0 ± 0.5
$E_{\mathrm{L\text{-}J}}$	–36.3 ± 5.4	–31.4 ± 4.9
Atomic r.m.s. differences (Å)[c]		
Backbone atoms (3–32)	0.18 ± 0.04	0.23 ± 0.10
Heavy atoms (3–32)	0.77 ± 0.09	0.83 ± 0.14

[a] Idealized geometry is defined by the CHARMM force field as implemented within X-PLOR.
[b] The final values of the square-well NOE and dihedral-angle potentials were calculated with force constants of 50 kcal mol^{-1} Å^{-2} and 200 kcal mol^{-1} Å^{-2}, respectively.
[c] Atomic r.m.s. differences are given as the average difference against the mean coordinate structure. All statistics are given as mean ± S.D.

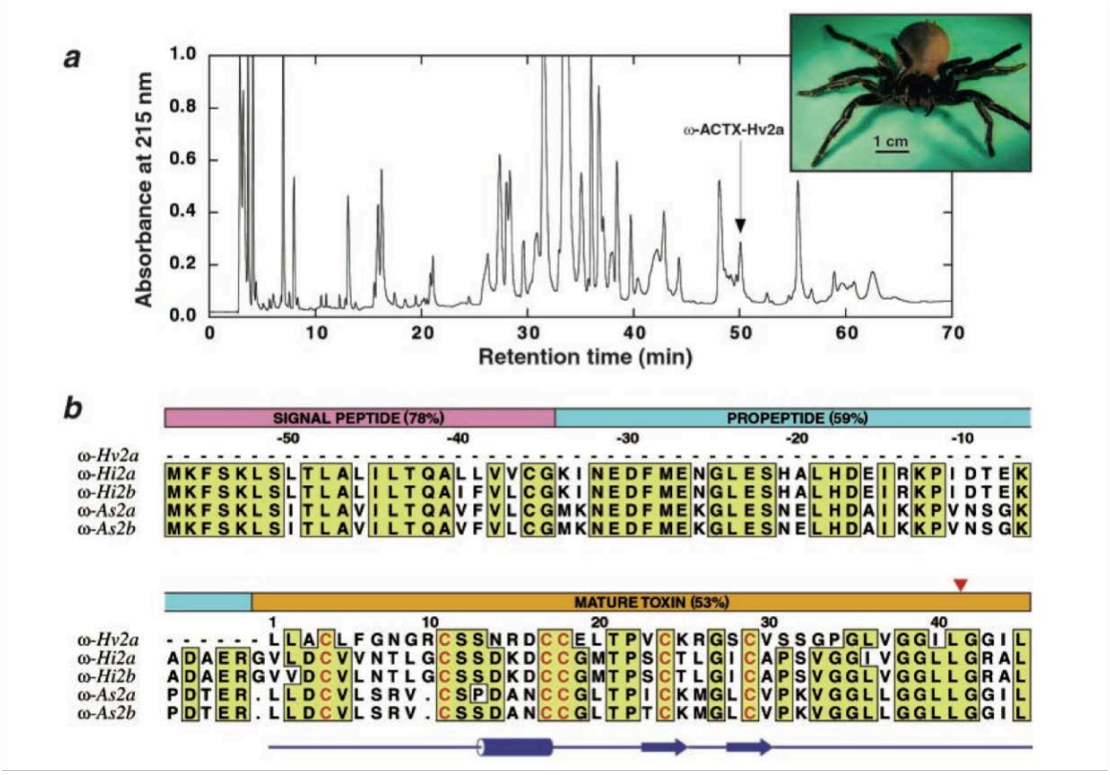

FIG. 1. Purification and primary structure of ω-atracotoxin-Hv2a. *a*, rpHPLC chromatogram of whole *H. versuta* venom. The *arrow* indicates the retention time of the insect-specific toxin ω-ACTX-Hv2a. The *inset* shows a female specimen of *H. versuta* in an aggressive/defensive "ready-to-strike" stance with forelegs and palps raised and fangs exposed. *b*, comparison of primary structures of ω-atracotoxins from *H. versuta* (ω-ACTX-Hv2a), *H. infensa* (ω-ACTX-Hi2a and ω-ACTX-Hi2b), and *Atrax* sp. Illawarra (ω-ACTX-As2a and ω-ACTX-As2b). The ω-ACTX-Hv2a sequence was derived from protein sequencing, whereas the other primary structures are inferred from cDNA sequences (see the text). Residues boxed in *yellow* are identical in four or more of the sequences, whereas the strictly conserved cysteine residues are highlighted in *red*. The signal, propeptide, and mature peptide regions of the prepropeptide are indicated, and the percentage of amino acid identity within each of these regions is given in parentheses. The *red arrowhead* marks the site of additional C-terminal processing of the *H. infensa* toxins (see the text). The secondary structure of ω-ACTX-Hv2a, as determined in the current study, is shown *below* the sequences (β-strands and 3_{10}-helices are depicted as *arrows* and *cylinders*, respectively).

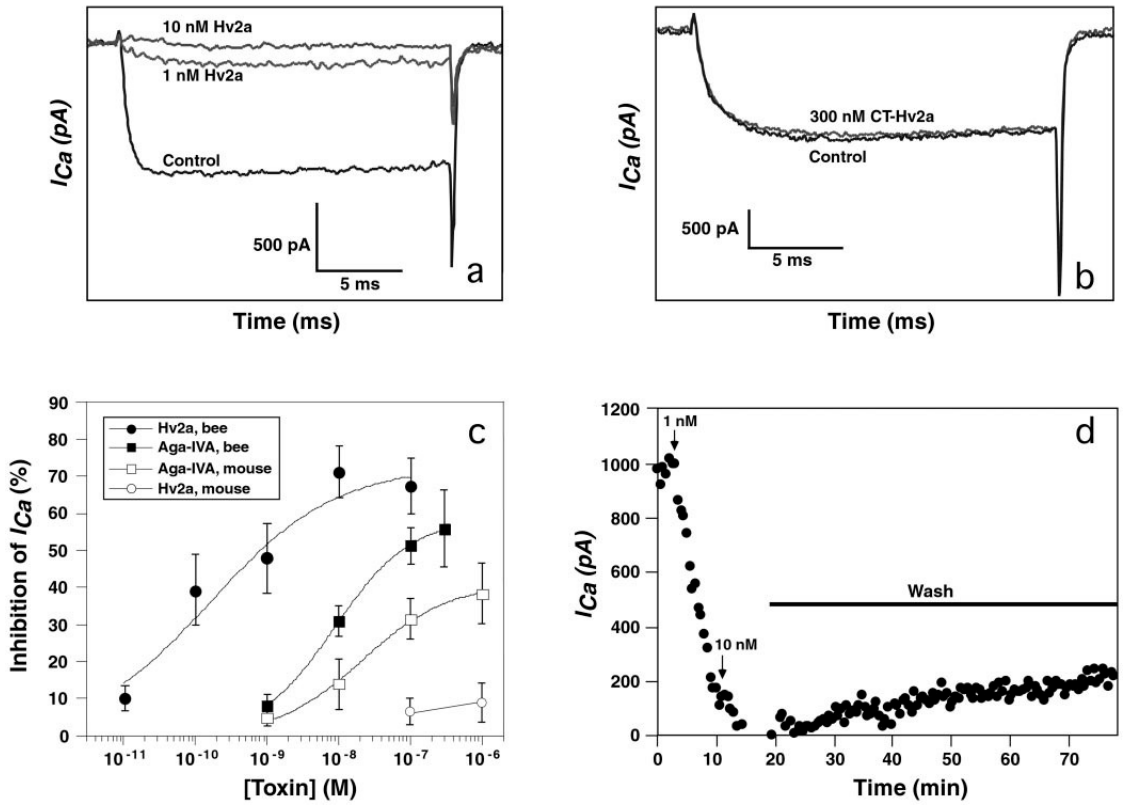

FIG. 2. ω-ACTX-Hv2a is a specific antagonist of insect voltage-gated calcium channels. *a*, whole cell calcium channel currents (I_{Ca}) recorded from a bee brain neuron in the absence (control) or presence of ω-ACTX-Hv2a. *b*, whole cell calcium channel currents recorded from a bee brain neuron in the absence (control) or presence of CT-Hv2a. *c*, dose-response curves for inhibition of I_{Ca} in bee brain and rat trigeminal neurons by ω-ACTX-Hv2a (closed and open circles) and ω-Aga-IVA (closed and open squares). Each data point is the mean ± S.D. of 7–10 recordings. The curves are the result of fitting a simple logistic function to the data. *d*, time course for inhibition of I_{Ca} recorded from a bee brain neuron after the addition of 1 and 10 nM ω-ACTX-Hv2a at the indicated times. Inhibition was rapid and was not significantly reversed by prolonged washing (indicated by the *horizontal bar*).

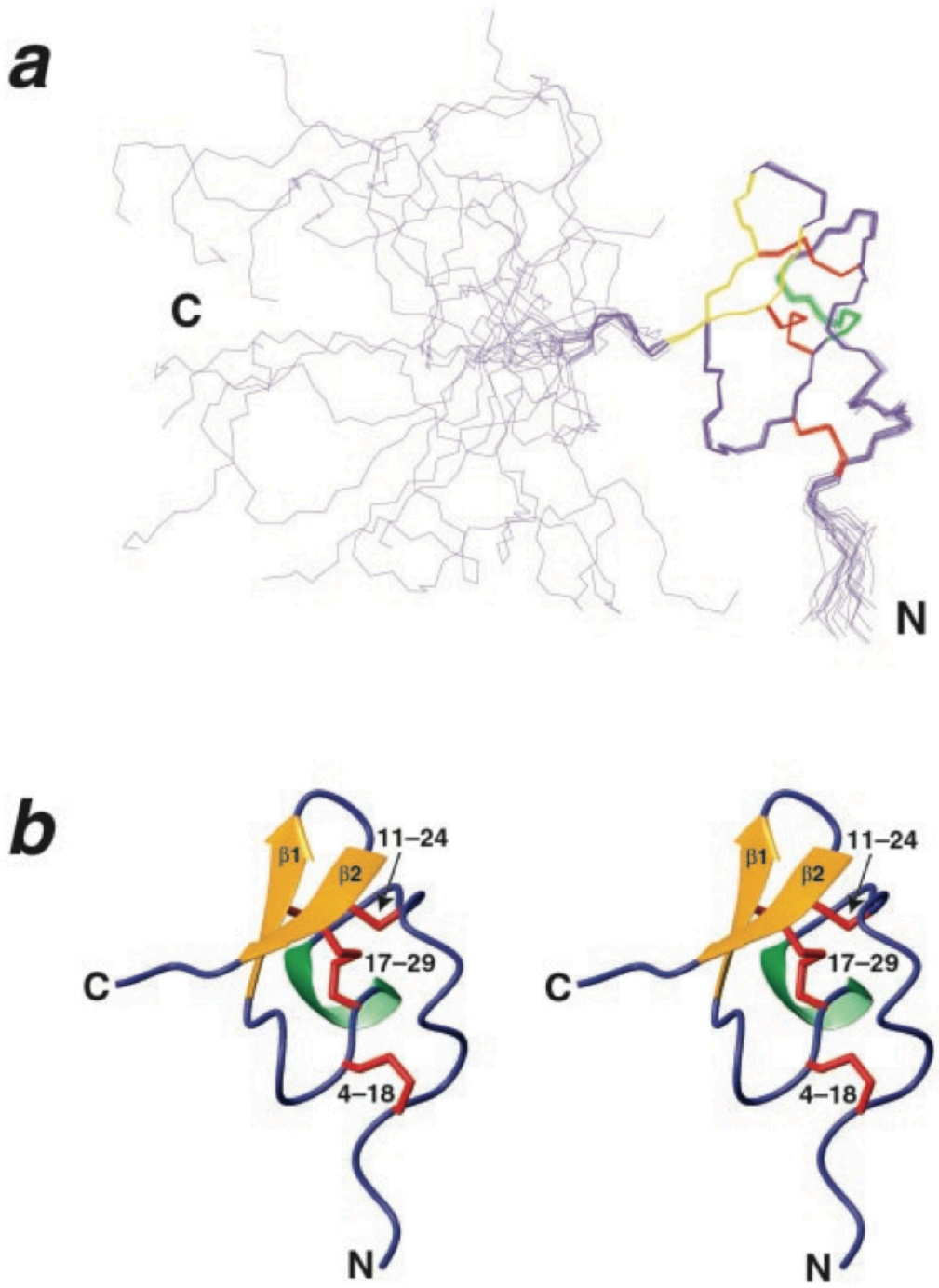

FIG. 3. Solution structure of ω-ACTX-Hv2a. *a*, ensemble of 20 ω-ACTX-Hv2a structures superimposed for best fit over the backbone atoms of residues 3–32 of the mean coordinate structure. Disulfide bonds are shown in *red*, and the backbone is colored *green* (3_{10}-helix), *gold* (β-strands), or *blue*. Note the unstructured C-terminal domain (residues 33–45). *b*, stereo view of the globular disulfide-rich domain (residues 1–32) with the same molecular orientation and color scheme as described in *a*. Disulfide bridges are labeled.

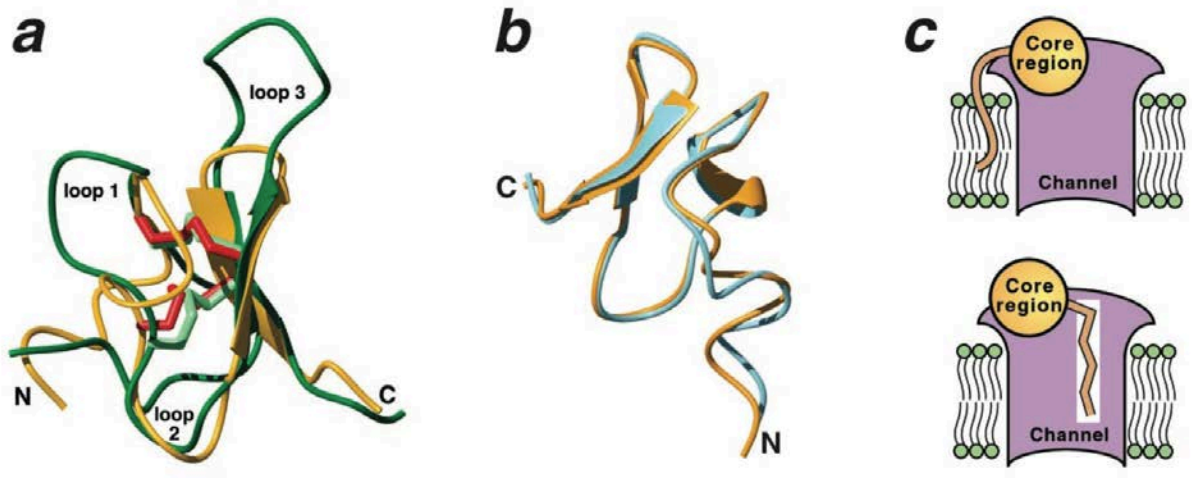

FIG. 4. *a*, overlay of ω-ACTX-Hv2a (*gold*) on ω-Aga-IVA (*green*; Protein Data Bank accession code 1OAW); the core disulfide bridges of each toxin are shown as *red* and *sage* tubes, respectively. A similar comparison can be made with ω-Aga-IVB (Protein Data Bank accession code 1AGG). The folds are homologous, but loops 1 and 3 are more highly elaborated in ω-Aga-IVA/B. The molecules are rotated ~180° around the long axis of the β-hairpin relative to the view in Fig. 3. *b*, the mean 20 CT-Hv2a structure (*cyan*) superimposed for best fit over the backbone of residues 3–32 of the mean ω-ACTX-Hv2a structure (*gold*). The molecular orientation is similar to that in Fig. 3. *c*, hypothetical models of the mechanism of action of ω-ACTX-Hv2a and ω-Aga-IVA in which the lipophilic C-terminal tail (*orange*) penetrates the lipid bilayer either adjacent to the channel (*top panel*) or by intercalation between transmembrane segments of the calcium channel (*bottom panel*). In either case, this positions the disulfide-rich core (*shaded sphere*) for direct interaction with the extracellular surface of the channel.